JOURNAL OF SOLID STATE CHEMISTRY 91, 105–112 (1991)

Crystal Structure, Short Range and Long Range Magnetic Ordering in $CuSb_2O_6$

A. NAKUA,* H. YUN,*,† J. N. REIMERS,* J. E. GREEDAN,* AND C. V. STAGER‡

*Departments of *Chemistry and ‡Physics and the Institute for Materials Research, McMaster University, Hamilton, Ontario, Canada L8S 4M1*

Received July 3, 1990; in revised form October 22, 1990

$CuSb_2O_6$ crystallizes in a monoclinically distorted trirutile structure. Atomic positions were determined by profile refinement of neutron powder diffraction data, space group $P2_1/n$, $a = 4.6349(1)$, $b = 4.6370(1)$, $c = 9.2931(1)$, $\beta = 91.124(2)$. Magnetic susceptibility data exhibit a broad maximum at about 60 K and an abrupt transition at 8.5 K. The high temperature data can be fitted to a Curie–Weiss Law giving $\mu_{eff} = 1.758$ and $\theta = -48$ K. Although the crystal structure indicates a nearly square planar Cu^{2+} lattice as in other trirutiles, a Cu–O–O–Cu superexchange pathway seems to be dominant, giving rise to short range correlations which are approximately one dimensional. The high-temperature susceptibility is explained well by the 1-d Heisenberg model with $J/k = -43.1$ K. Analysis by Oguchi's method gives a ratio of interchain to intrachain coupling constants of about 2×10^{-3}.

Introduction

Antimonates and tantalates of the type $M^{II}Sb_2(Ta_2)O_6$ have been studied extensively in this laboratory (*1–5*). It was reported previously that $CuSb_2O_6$ crystallizes in a distorted monoclinic trirutile structure in space group $P2_1/c$ or $P2_1/n$, but a detailed crystal structure analysis has not been reported (*6–9*). The trirutile structure type, Fig. 1, can be generated from the rutile structure by tripling the c-axis due to the chemical ordering of the divalent and pentavalent cations. The structure consists of a network of edge and corner sharing CuO_6 and SbO_6 octahedra. The Cu^{2+} and Sb^{5+} cation positions are such that the magnetic Cu^{2+} ions are separated from each other by two sheets of diamagnetic ions. In fact, the magnetic cation sublattice is the same as that of the K_2NiF_4 structure, which is a canonical example of a square lattice two-dimensional antiferromagnet. Considering the in-plane superexchange pathways, the dominant interaction appears to occur through a linear Cu–O–O–Cu linkage which connects one set of two next nearest neighbor Cu^{2+} ions. Interestingly, the superexchange pathways to the other two next nearest neighbor ions are not equivalent, involving Cu–O–Cu linkages with long, 3.6 Å, bonds and a 160° bond angle (*1*). Thus, it is possible to think of one-dimensional in-plane interactions and this is aided by the fact that the Cu–O–O–Cu chains are translated by $\frac{1}{2}\langle 110\rangle$ with respect to each other giving rise

† Present address: Korea Institute of Science and Technology, P.O. Box 131, Cheongryang, Seoul, Korea.

0022-4596/91 $3.00

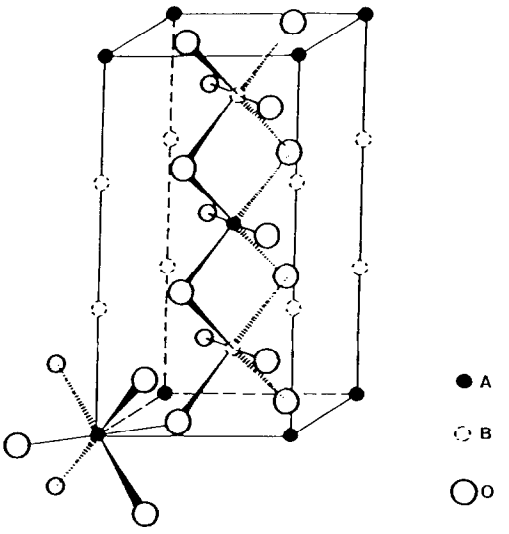

FIG. 1. The trirutile structure.

to frustrated interchain coupling as pictured in Fig. 2.

The magnetic properties of $CuSb_2O_6$ have been reported in the temperature range above 90 K (*8*). In the interval 90 to 300 K the data were fitted to a Curie–Weiss law with $\mu_{eff} = 1.1_{\mu B}$ and $\theta_c = -50(10)$ K. Data at higher temperatures showed an anomaly near 500 K which corresponds to a monoclinic to tetragonal structural transition.

In this work, new results on $CuSb_2O_6$ are presented including a structural refinement using neutron powder profile techniques and magnetic susceptibility data down to 2 K. An effort is made to model the observed susceptibility in terms of short range interactions.

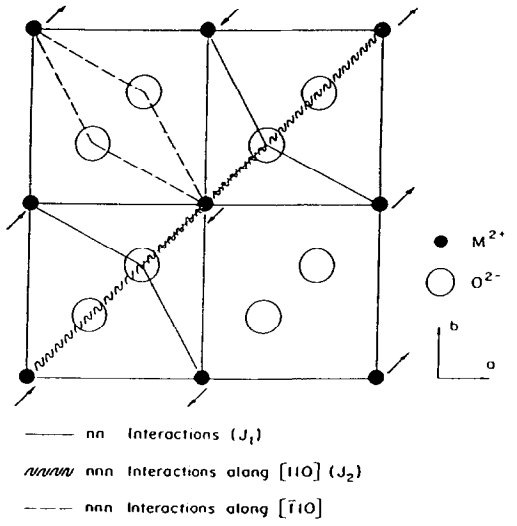

FIG. 2. In-plane superexchange pathways in the trirutile structure.

Experimental

Preparation

$CuSb_2O_6$ was prepared by the reaction of CuO (Johnson-Matthey) and Sb_2O_3 (Baker) in air at 1000°C. In order to minimize volatilization of Sb_2O_3 the reactants were heated at a rate of 4°C/min. The yellow color of the product is consistent with the previous reports. Complete reaction was verified by X-ray powder diffraction. The purity of the sample was very dependent on the pressure used for the pelletization. Pressures higher than 2×10^4 psi resulted in the formation of another phase on the pellet surface identified as $Cu_4SbO_{4.5}$ (*9*).

X-Ray Powder Diffraction

Powder data were obtained in the range $10 < 2\theta < 80°$ using a Nicolet I2 diffractometer.

Powder Neutron Diffraction

Neutron diffraction data were collected at room temperature on the General Purpose Powder Diffractometer (GPPD) at the Intense Pulsed Neutron Source (IPNS) at Argonne National Laboratory (*10*). A general discussion of the time-of-flight (TOF) method regarding operation principles, peak shape and background analysis methods, and specific information on the GPPD at IPNS has been given previously (*11*). Data were collected from the $2\theta = 148°$, 90°, and

TABLE I

SUMMARY OF INTENSITY COLLECTION AND RIETVELD REFINEMENT RESULTS FROM NEUTRON DATA FOR $CuSb_2O_6$

a (Å)	4.6349(1)
b (Å)	4.6370(1)
c (Å)	9.2931(10)
β (degrees)	91.124(2)
V (Å^3)	199.69
Space group	C_{2h}^5–$P2_1/n$
T of data collection (K)	298
Detector bank (2θ, degrees)	148
d-spacing, limits (Å^{-1})	0.53–2.13
No. of observations	2819
No. of reflections	1442
No. of variables	31
R_p^a	0.050
R_{wp}^a	0.072
R_B^a	0.013
R_B^a	0.047

[a] Ref. (*1*).

60° detector banks, but only backscattering data (2θ = 148°) were used in the refinement so as to achieve the highest possible resolution. Data preparation and least squares refinement were carried out using the programs of the IPNS Rietveld analysis package for TOF data from spallation pulsed neutron sources (*12*). Details on the data collection and refinement results are given in Table I.

Magnetic Susceptibility

Magnetic susceptibility data were collected on a Quantum Design SQUID magnetometer using a pressed polycrystalline pellet. The magnetometer was calibrated with a high purity palladium sample.

Results and Discussion

Structure Data

The cell parameters were taken from reference (*7*) and the starting positional parameters for the refinement were derived from the tetragonal $ZnSb_2O_6$ structure (*6*). The final refinement in space group $P2_1/n$ included 2819 observations and 1442 independent reflections (0.53 Å $\leq d \leq$ 2.13 Å). The 31 variables refined included a scale factor, cell parameters, positional parameters, isotropic thermal parameters, an absorption parameter, and background and profile parameters. The final agreement indices are R_p = 0.050, R_{wp} = 0.072. The statistically expected weighted profile R_E = 0.013. Figure 3 shows the final Rietveld profile fit for $CuSb_2O_6$. Atomic parameters along with isotropic thermal parameters and some bond angles and distances are given in Table II and Table III, respectively.

TABLE II

ATOMIC PARAMETERS FOR $CuSb_2O_6$

Atom	Site	x	y	z	B(Å^2)
Cu	2*a*	0	0	0	0.21(6)
Sb	4*e*	0.0011(9)	0.0080(10)	0.3338(6)	0.16(4)
O1	4*e*	0.3130(9)	0.2983(8)	0.0017(4)	0.13(5)
O2	4*e*	0.2991(8)	0.3176(7)	0.3291(4)	0.36(6)
O3	4*e*	−0.3012(8)	−0.2915(9)	0.3248(4)	0.63(7)

TABLE III

SELECTED BOND DISTANCES (Å) AND ANGLES (DEGREES) FOR $CuSb_2O_6$

Cu–2O(1)	2.004(4)	2O(1)–Cu–O(2)	92.27(15)
Cu–2O(2)	2.012(4)	2O(1)–Cu–O(3)	90.28(16)
Cu–2O(3)	2.120(4)	2O(2)–Cu–O(3)	102.31(15)
Sb–O(1)	2.013(7)	O(1)–Sb–O(1)	79.07(27)
Sb–O(1)	1.994(6)	O(1)–Sb–O(2)	90.36(25)
Sb–O(2)	1.993(6)	O(1)–Sb–O(2)	177.99(33)
Sb–O(2)	1.996(6)	O(1)–Sb–O(3)	91.67(25)
Sb–O(3)	1.973(6)	O(1)–Sb–O(2)	99.52(25)
Sb–O(3)	1.960(6)	O(1)–Sb–O(2)	94.52(25)
		O(1)–Sb–O(3)	99.55(25)
		O(1)–Sb–O(3)	89.15(25)
		O(2)–Sb–O(2)	177.39(33)
		O(2)–Sb–O(3)	88.28(21)
		O(2)–Sb–O(3)	176.09(36)
		O(2)–Sb–O(3)	87.68(25)
		O(2)–Sb–O(3)	89.77(25)
		O(3)–Sb–O(3)	81.91(26)
			88.69(21)

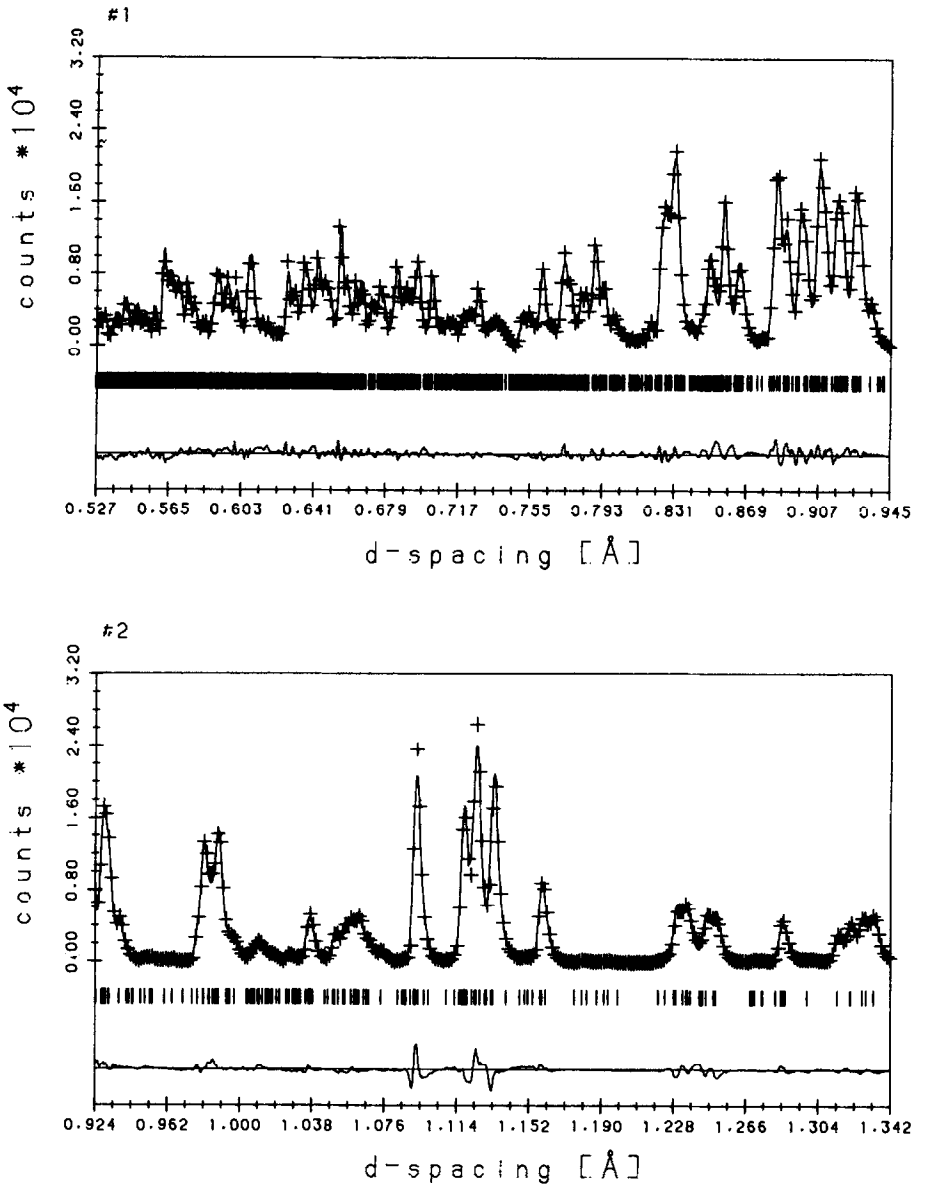

FIG. 3. Neutron powder profile data and fit for $CuSb_2O_6$. The crosses represent profile points, the solid line is the calculated profile, and the difference is plotted below.

Magnetic Susceptibility

Magnetization and inverse susceptibility data at an applied field of 200 Oe are shown in Figs. 4 and 5.

The magnetization data show a broad maximum at about 60 K which is indicative of short range order and a sharp decrease at 9 K suggesting a long range order transition. Magnetic data from 5 to 340 K were

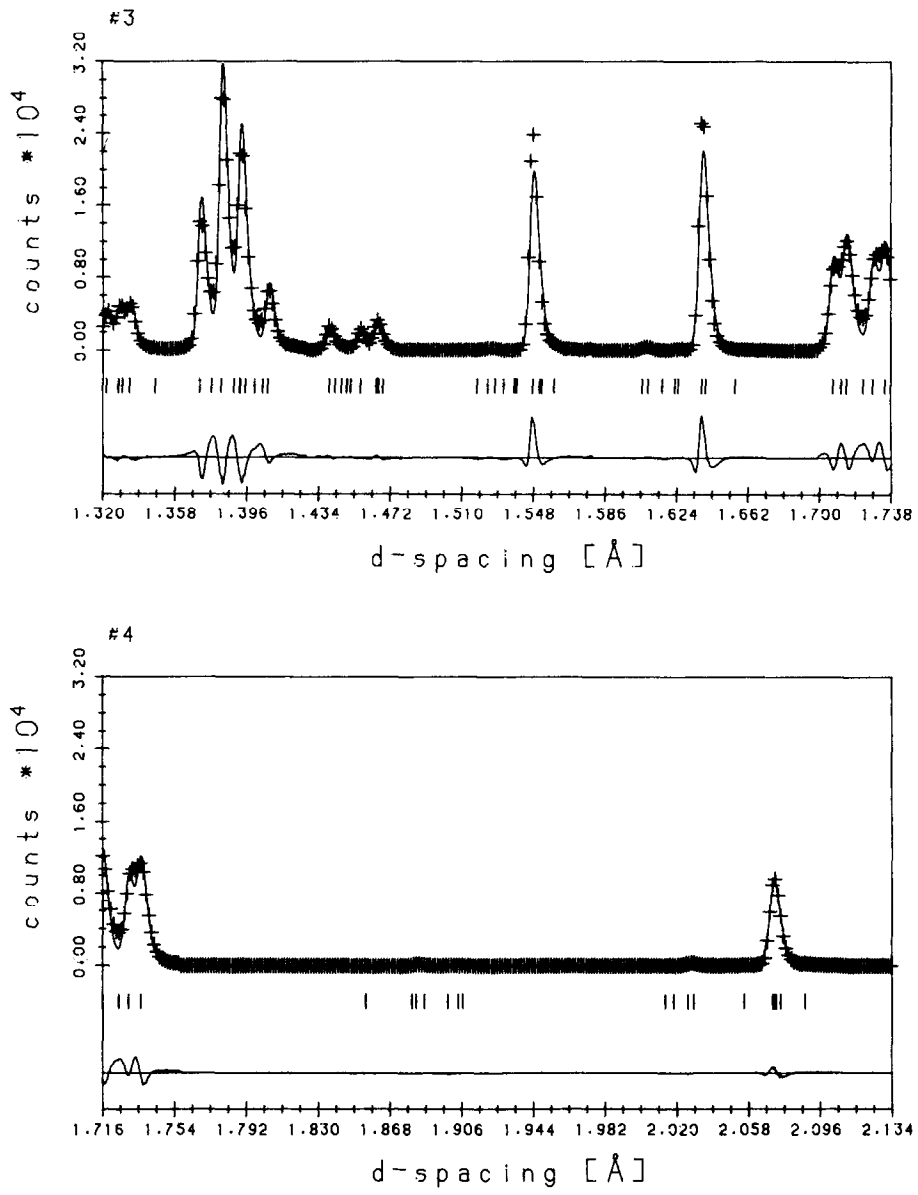

FIG. 3. *Continued.*

fitted to a Curie–Weiss law after correction for diamagnetism, $\chi_{corr}^{-1} = (T - \theta_c)/c_M$ giving $\mu_{eff} = 1.758$ and $\theta = -48$ K in fair agreement with previous work [8]. The inverse susceptibility data below 150 K deviate considerably from the Curie–Weiss law due to short range order. The susceptibility attains a maximum value of 2.7×10^{-2} cm^3 mol^{-1} at 60 K.

It is possible to analyze the data of Fig. 4 by the method suggested by Fisher (*13*) to obtain an approximation to the magnetic

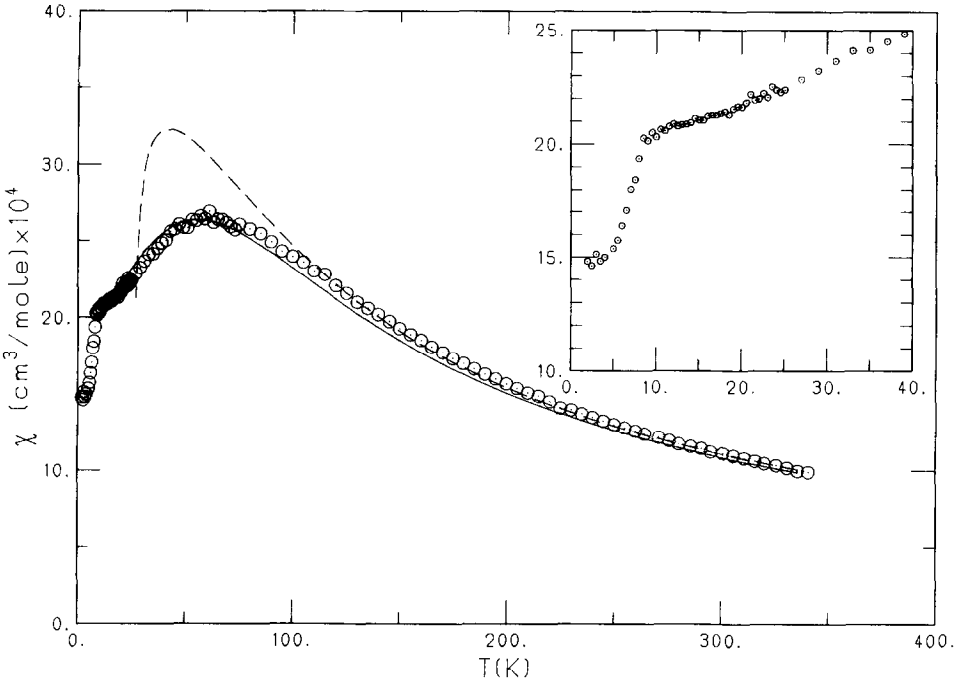

FIG. 4. Magnetic susceptibility versus temperature for $CuSb_2O_6$ at an applied field of 200 Oe compared with two $S = \frac{1}{2}$ Heisenberg models: linear chain (——) square lattice (---). The inset shows the abrupt transition at 8.5 K.

specific heat. A plot, Fig. 6, of $d(\chi T)/dT$ shows two features, a broad maximum at about 40 K and a sharp spike at 9 K. The latter feature is likely a transition to a long range ordered state. Further evidence for this is found in Fig. 7, where magnetic moment versus applied field data are plotted at 2 and 11 K. At 2 K, below T_c, the curve shows two linear regimes, 0.0 to about $1T$ and 2.0 to $3.0T$ with a transition region in between. This behavior is characteristic of a spin flop transition in polycrystalline samples. The 11 K data on the other hand are linear throughout the entire field range which is typical of the paramagnetic state. Preliminary neutron diffraction data taken at 4.2 K showed no sign of magnetic reflections, indicating that the copper magnetic moment may be less than one Bohr magneton. These measurements will be repeated at a high flux neutron source.

The data of Fig. 6, while not quantitative, indicate that a large magnetic heat capacity contribution persists well above T_c, which is

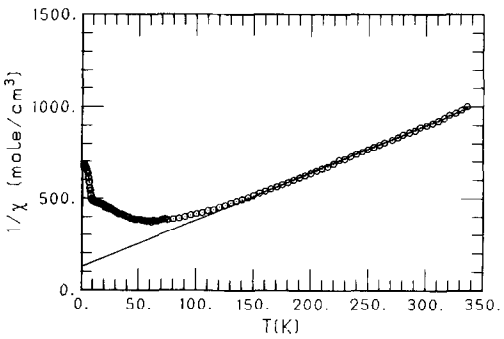

FIG. 5 Inverse susceptibility data for $CuSb_2O_6$.

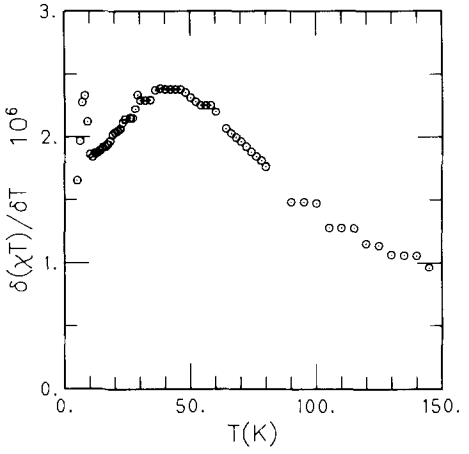

FIG. 6. Fisher's heat capacity for $CuSb_2O_6$.

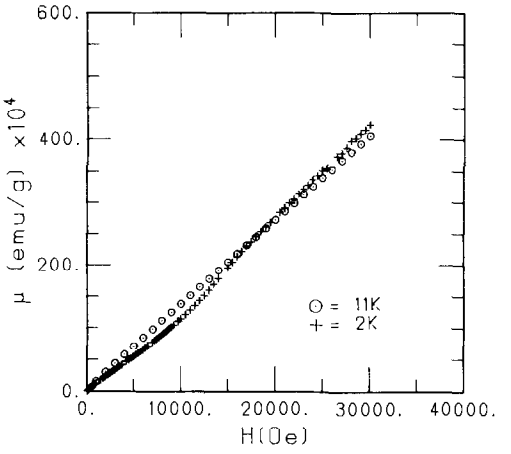

FIG. 7. Magnetic moment versus applied field for $CuSb_2O_6$ at 2 K and 11 K.

characteristic of short range order. A more quantitative characterization of the short range order can be obtained through analysis of the magnetic susceptibility data. Cu^{2+} is generally regarded as an excellent $S = \frac{1}{2}$ Heisenberg ion as the ground state anisotropy is very small. Thus, relatively little is lost by working with polycrystalline data.

Two models were used to fit the susceptibility data in the range from about 10 to 340 K. First, following the arguments put forward in the introduction an $S = \frac{1}{2}$ Heisenberg linear chain model was used in the form of the analytic expression suggested by Hall (*14*). The fit which uses only two adjustable parameters, g and J the exchange constant, is shown in Fig. 4. The result is surprisingly good with the values $g = 2.03$ and $J/k = -43$ K. A fit to a square lattice $S = \frac{1}{2}$ Heisenberg model was also attempted based on the high temperature series expansion by Rushbrooke and Wood (*15*). The results are also shown in Fig. 4 and the fit with the parameters $g = 2.03$ and $J/k = -22.6$ K is clearly worse than for the linear chain model. Thus, the linear chain model is a better approximation to the short range order in $CuSb_2O_6$ than the square lattice.

It is instructive to compare the known results for other members of the $M^{II}Ta_2(Sb_2)O_6$ series with those for $CuSb_2O_6$ as in Table IV. The $CuSb_2O_6$ phase stands out in two categories, largest $T(\chi_{max})/T_c$ ratio of 7.1 and largest dominant in-plane exchange constant $J/k = -43$ K. The $T(\chi_{max})/T_c$ ratio can be taken as a crude measure of the relative importance of short range versus long range correlations. This is because the intrachain coupling constant, J, is proportional to $T(\chi_{max})$, the proportionality constant being model dependent, while T_c

TABLE IV

RELEVANT MAGNETIC DATA FOR $M^{II}Ta_2(Sb_2)O_6$ COMPOUNDS

Compound	$T(\chi_{max})$ (K)	T_c(K)	$\frac{T(\chi_{max})}{T_c}$	Dominant in-plane exchange J/k (K)	Ref.
$FeTa_2O_6$	15	8.1	1.7	−16	(*1*)
$CoTa_2O_6$	15.6	6.6	2.3	−16.8	(*2, 3*)
$CoSb_2O_6$	35	13.0	2.7	—	(*4*)
$NiTa_2O_6$	25	10.3	2.4	−15	(*2, 3*)
$NiSb_2O_6$	36	—	—	—	(*16*)
$CuSb_2O_6$	60	8.5	7.1	−43	

is related to J^1, the interchain constant. de Jongh and Miedema (*17*) have shown that the Oguchi relationship (*18*) gives a reasonable estimate of J^1/J from T_c and $|J|$. On this basis $J^1/J \sim 2 \times 10^{-3}$ for $CuSb_2O_6$, which is comparable to other Cu^{2+} compounds generally regarded as good examples of linear chain behavior (*17*). Of all the known $MTa_2(Sb_2)O_6$ trirutile oxides $CuSb_2O_6$ shows the clearest evidence yet for the dominance of one-dimensional correlations in the short range ordered regime.

Acknowledgments

We thank G. Hewitson for assistance in obtaining the magnetic susceptibility data. The financial support of the Natural Science and Engineering Research Council of Canada is acknowledged.

References

1. S. M. Eicher, J. E. Greedan, and K. J. Lushington, *J. Solid State Chem.* **62,** 220 (1986).
2. R. K. Kremer and J. E. Greedan, *J. Solid State Chem.* **73,** 579 (1988).
3. R. K. Kremer, J. E. Greedan, E. Gmelin, W. Dar, and M. A. White, *J. Phys. C* **49,** C8–1495 (1988).
4. J. N. Reimers, J. E. Greedan, and M. A. Subramanian, *J. Solid State Chem.* **79,** 263 (1989).
5. J. N. Reimers, J. E. Greedan, C. V. Stager, and R. K. Kremer, *J. Solid State Chem.* **83,** 20 (1989).
6. A. Bystrom, B. Hok, and B. Mason, *Ark. Kemi Mineral. Geol.* **15B,** 1 (1941).
7. NBS Report No. 9086, JCPDS Card No. 17-284.
8. J. D. Donaldson, A. Kjekshus, D. G. Nicholson, and T. Rakke, *Acta Chem. Scand. Ser. A* **29,** 803 (1975).
9. S. Shimada and K. J. D. Mackenzie, *Thermochim. Acta* **56,** 73 (1982).
10. J. Jorgensen and F. Rotella, *J. Appl. Crystallogr.* **15,** 27 (1982).
11. S. McEwen, J. Faber, Jr., and A. Turner, *Acta Metall.* **31,** 657 (1983).
12. R. von Dreele, J. Jorgensen, and C. Windsor, *J. Appl. Crystallogr* **15,** 581 (1982).
13. M. E. Fisher, *Phil. Mag.* **17,** 1731 (1962).
14. J. W. Hall, Ph.D. Dissertation, The University of North Carolina at Chapel Hill, Chapel Hill (1977); W. E. Hatfield, *J. Appl. Phys.* **52,** 1985 (1981).
15. G. S. Rushbrooke, and P. J. Wood, *Mol. Phys.* **1,** 257 (1958) and *Mol. Phys.* **6,** 409 (1963).
16. J. N. Reimers and J. E. Greedan, unpublished.
17. L. J. de Jongh and A. R. Miedema, *Adv. Phys.* **23,** 1 (1974).
18. T. Oguchi, *Phys. Rev. A* **133,** 1098 (1964).